

## Article

# RETRACTED: Preparation and Analysis of Structured Color Janus Droplets Based on Microfluidic 3D Droplet Printing

Chuang Wu <sup>1,\*</sup>, Hanqi Jia <sup>1</sup>, Haithm Yahya Mohammed Almuaalemi <sup>1</sup>, A. S. M. Muhtasim Fuad Sohan <sup>2</sup>  
and Binfeng Yin <sup>1,\*</sup>

<sup>1</sup> School of Mechanical Engineering, Yangzhou University, Yangzhou 225127, China; mz120230875@stu.yzu.edu.cn (H.J.); mh22012@stu.yzu.edu.cn (H.Y.M.A.)

<sup>2</sup> School of Electrical and Mechanical Engineering, The University of Adelaide, Adelaide, SA 5005, Australia; asmmuhtasimfuad.sohan@student.adelaide.edu.au

\* Correspondence: 007511@yzu.edu.cn (C.W.); binfengyin@yzu.edu.cn (B.Y.)

**Abstract:** The microfluidic technique for the three-dimensional (3D) printing of Janus droplets offers precise control over their size, orientation, and positioning. The proposed approach investigates the impact of variables such as the volume ratio of the oil phase, droplet size, and the ratio of nonionic surfactants on the dimensions of the structured color apertures of Janus droplets. The findings reveal that structured color apertures modulate accurately. Furthermore, fabricating color patterns facilitates cat, fish, and various other specific shapes using structured color Janus droplets. The color patterns exhibit temperature-sensitive properties, enabling them to transition between display and concealed states. Herein, the adopted microfluidic technique creates Janus droplets with customizable characteristics and uniform size, solving orientation as well as space arrangement problems. This approach holds promising applications for optical devices, sensors, and biomimetic systems.

**Keywords:** microfluidic technology; structural color; Janus droplet; temperature-sensitive characteristics; hydrogel



**Citation:** Wu, C.; Jia, H.; Almuaalemi, H.Y.M.; Sohan, A.S.M.M.F.; Yin, B. RETRACTED: Preparation and Analysis of Structured Color Janus Droplets Based on Microfluidic 3D Droplet Printing. *Micromachines* **2023**, *14*, 1911. <https://doi.org/10.3390/mi14101911>

Academic Editor: Xiangsong Feng

Received: 10 September 2023

Revised: 5 October 2023

Accepted: 5 October 2023

Published: 7 October 2023

Retracted: 28 March 2024



**Copyright:** © 2023 by the authors. Licensee MDPI, Basel, Switzerland. This article is an open access article distributed under the terms and conditions of the Creative Commons Attribution (CC BY) license (<https://creativecommons.org/licenses/by/4.0/>).

## 1. Introduction

In the development processes of production and life, functional composite materials gradually occupy an important position in fields such as medicine, optics, functional displays, and biological manufacturing due to their complex chemical composition, multiple physical structures, and diverse functions [1,2]. Single-component materials generally have problems such as a simple physical structure, lack of functionality, single chemical composition, and inability to meet the needs of high-precision production [3,4]. Compared to single-component materials, functional composite materials Janus droplets have excellent comprehensive performance characteristics, making them have broad application prospects [5,6].

Structural color is a physical phenomenon arising from the precise alignment of atomic or molecular spacing within a material with the wavelengths of visible light. This phenomenon manifests as visually stunning and exhibits remarkable color stability and environmentally sustainable characteristics [7,8]. Janus droplets typically consist of materials exhibiting distinct chemical or physical properties, and their dimensions consistently fall within the range of microns or nanometers [9,10]. The anisotropic structure of Janus droplets is not only reflected in the non-pairing of chemical composition or morphological structure, but also in the non-pairing of function or performance [11,12]. When Janus droplets are composed of two liquids with different refractive indexes, the incident light can interfere at the interface, resulting in a gorgeous ring pattern, that is, structural color. Therefore, Janus droplets with a structured color have important application value in optics, displays, anti-counterfeiting materials, and other fields [13–15]. The density of n-hexane

(C<sub>6</sub>H<sub>14</sub>) is 0.66 g/cm<sup>3</sup>; it is insoluble in water and has a refractive index of 1.372 [16,17]. Perfluorohexane (C<sub>6</sub>F<sub>14</sub>) has a density of 1.68 g/cm<sup>3</sup>, is insoluble in water, and has a refractive index of 1.252 [18,19]. At room temperature, n-hexane and perfluorohexane are not miscible, but have a unique temperature sensitivity; that is, they have a critical mutual solubility temperature of 23 °C. When heated to above 23 °C, the two oil phases are miscible, while when cooled to below 23 °C, the two are immiscible and immediately delaminate [20,21]. Due to the physical and chemical properties of n-hexane and perfluorohexane that meet the conditions for preparing structural colored Janus droplets, this article intends to use these two materials as the main raw materials to prepare structural colored Janus droplets.

In microfluidic 3D droplet printing, droplets are continuously discrete and extruded from a printing nozzle in a bath filled with a supporting substrate. The supporting substrate generally adopts a shear-thinned hydrogel [22–24]. Carbomer 940 is a polymer obtained via the copolymerization of a monomer and crosslinking agent, which is white and fluffy, and its aqueous solution is acidic. It is a viscous hydrogel when neutralized with an alkaline solution [25,26]. Carbomer hydrogels have excellent shear-thinning characteristics. When the printing nozzle moves rapidly in a carbomer hydrogel, the local liquefaction of the hydrogel enables the nozzle to move easily and shear droplets. With the passage of the nozzle, the partially liquefied hydrogel returns to a stable hydrogel state. This process suspends the droplets in a fixed position. Since the properties of carbomer hydrogels meet the requirements, this paper plans to select a carbomer hydrogel as the support matrix material for microfluidic 3D droplet printing.

A surfactant is a substance with an amphiphilic molecular structure, which has both hydrophilic and lipophilic properties. They can adjust the surface tension of the solution [27–29]. Selecting suitable surfactants is imperative to enhance the interfacial tension between oil-phase materials like n-hexane, perfluorohexane, and carbomer hydrogels. Suitable material can effectively manipulate the interfacial morphology of structured color Janus droplets, enabling precise control over their preparation. The inclusion of ionic surfactants in this context poses a potential issue. Ionic surfactants introduce an electric charge, which can disrupt the integrity of the carbomer hydrogel, rendering it incapable of supporting the formation of Janus droplets [30,31]. Nonionic surfactants Capstone FS-30 (FS-30) and Triton X-100 (X-100) have excellent emulsifying and wetting properties. They can adjust the interfacial tension, thus forming Janus droplets with stable interfacial morphology [32,33]. Therefore, in this paper, non-ionic surfactants FS-30 and X-100 will be selected as the regulating materials of interfacial tension between n-hexane/perfluorohexane and a carbomer hydrogel to prepare structural color Janus droplets with excellent performance.

Microfluidic technology is a scientific technology to control and operate fluids in micron-scale chip space, which has the advantages of low cost, simple operation, and high precision [34–38]. At present, microfluidic technology is commonly used to prepare small-volume Janus droplets composed of two or more materials with different chemical properties and physical structures. This method can generate droplets quickly and in large quantities while maintaining the uniformity of droplet size [39,40]. However, this technology cannot control the spatial orientation and position distribution of Janus droplets, and its manufacturing ability for macroscopic Janus droplets is relatively weak [41,42]. 3D printing technology is a rapid prototyping technology that directly converts the size information of a model into complex spatial structures. It has the advantages of free design, high-precision manufacturing, and maximizing material utilization, making it the preferred method for manufacturing complex 3D models. In response to the problems in the preparation of Janus droplets using microfluidic technology, this article combines 3D printing technology with microfluidic technology and successfully achieves a structurally colored Janus droplet with controllable size, position, and spatial orientation through an improved 3D printing device.

In this paper, structural color Janus droplets were prepared using microfluidic 3D droplet printing technology and a temperature-induced phase separation method, using a carbomer hydrogel containing non-ionic surfactant (FS-30/X-100) as a support matrix

and n-hexane and perfluorohexane as printing materials. The obtained Janus droplets can be flexibly adjusted in terms of size, proportion, orientation, position, and structural color, and can generate various color patterns composed of Janus droplets. The color patterns have temperature-sensitive properties and can be switched between display and hidden states, making them highly applicable.

## 2. Materials and Methods

### 2.1. Materials

Kapom 940, deionized water, sodium hydroxide, n-hexane, perfluorohexane, and X-100 were purchased from Aladdin Biochemical Technology, Shanghai, China. FS-30 was purchased from DuPont, Wilmington, DE, USA.

### 2.2. Methods

#### 2.2.1. Preparation of Janus Droplets with Structural Color

Step 1 involves the preparation of the supporting matrix, where Carbomer 940, FS-30, and X-100 are combined and dissolved in deionized water at 50 °C. The solution contains 0.075 wt% of carbomer, 1.5 wt% of FS-30, and 0.05 wt% of X-100. The solution is initially acidic, and then 10 wt% of NaOH solution is added to neutralize its pH. Finally, any remaining bubbles are eliminated in a vacuum box to yield a carbomer hydrogel, which serves as the supporting matrix for microfluidic 3D droplet printing.

In Step 2, the printing materials are prepared by mixing n-hexane and perfluorohexane at 24 °C, adhering to a volume ratio of 3:7. This results in a mutually soluble mixed solution. The ambient temperature within the printing system is maintained at 24 °C to ensure the two-phase solution remains mutually soluble throughout the printing process.

Step 3 involves the actual printing of Janus droplets. The 3D droplet printer was modified from the purchased 3D printer (Aurora Volvo A8L, Shenzhen Aurora Volvo Technology Co., Ltd., Shenzhen, China) (as shown in Figure 1). Take the hydrogel in step 1 as the substrate and place it on the lifting platform of the 3D droplet printer. Then, immerse the print nozzle in the carbomer hydrogel, generate the G code of the print path through Solidworks® version 2021 software (Dassault Systèmes SolidWorks Corporation, Waltham, MA, USA), and import it into the printer to start printing. During the printing process, the printer seamlessly adapts various parameters such as the feed rate, X/Y/Z axis movement speed, pause time, and more for the microinjection pump (LSP01-2A, Baoding Dichuang Electronic Technology Co., Ltd., Baoding, China), all based on the instructions encoded in the G code. This dynamic adjustment enables precise control over droplet size and positioning throughout the printing operation.

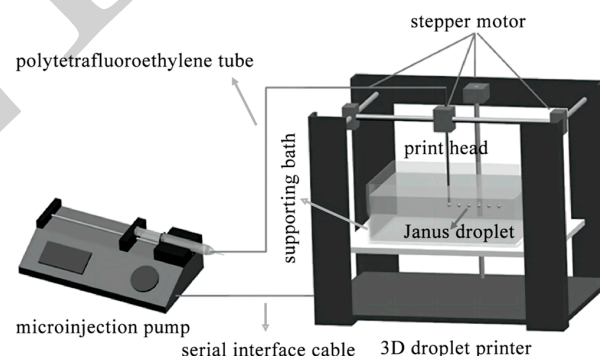


**Figure 1.** Schematic diagram of 3D droplet printer.

Step 4 involves the phase separation stage. Here, the support bath containing the droplets printed in Step 3 is carefully transferred to a refrigerated environment set at 8 °C. Over a certain duration, n-hexane and perfluorohexane within the droplets will naturally undergo phase separation. This separation results in the lighter-density n-hexane settling

in the upper layer, while the denser perfluorohexane occupies the lower layer. Consequently, this process forms Janus droplets, each oriented vertically in space, representing a significant outcome of this phase separation process.

The preparation process of structured color Janus droplets is visually detailed in Figure 2.

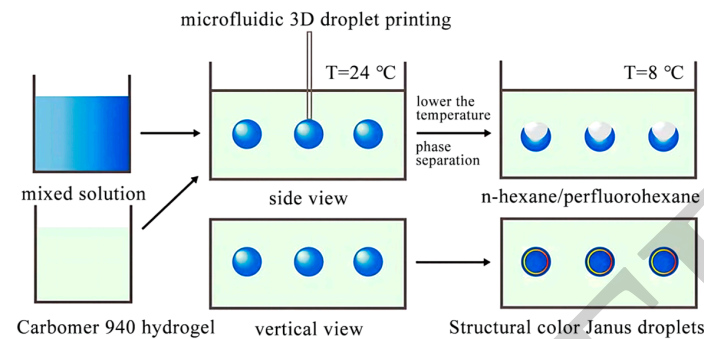


**Figure 2.** Schematic diagram of preparation process of structured color Janus droplets.

### 2.2.2. Influence of Volume Ratio of the Oil Phase

Janus droplets are composed of two oil phases, n-hexane and perfluorohexane, with structural colors occurring near the three-phase contact line. In order to verify the effect of the ratio of n-hexane-to-perfluorohexane on the structural color aperture, seven control experiments were set up, with the oil phase volume ratios of n-hexane and perfluorohexane as variables and the nonionic surfactants and droplet diameter as constants. The experiments were sorted according to the large and small oil phase volume ratio (as shown in Table 1). The concentration of FS-30 was 1.5 wt%, the concentration of X-100 was 0.05 wt%, and the droplet diameter was 0.569 mm.

**Table 1.** Experimental grouping of oil phase volume ratio.

Group	Oil Phase Volume Ratio (n-Hexane/Perfluorohexane)	Diameter (mm)	FS-30 (wt%)	X-100 (wt%)
1	19:11 (1.727)	0.569	1.5	0.05
2	3:2 (1.5)	0.569	1.5	0.05
3	17:13 (1.308)	0.569	1.5	0.05
4	8:7 (1.143)	0.569	1.5	0.05
5	1:1 (1.0)	0.569	1.5	0.05
6	13:17 (0.765)	0.569	1.5	0.05
7	11:19 (0.579)	0.569	1.5	0.05

### 2.2.3. Influence of Droplet Size

Seven control experiments were set up, with the droplet diameter as a variable and the volume ratio of nonionic surfactants-to-oil phase as a constant. The experiments were sorted based on the smallest to largest droplet diameters (as shown in Table 2). The concentration of FS-30 was 1.5 wt%, the concentration of X-100 was 0.05 wt%, and the volume ratio of n-hexane-to-perfluorohexane was 3:7.

**Table 2.** Experimental grouping of different droplet diameters.

Group	Diameter (mm)	Oil Phase Volume Ratio (n-Hexane/Perfluorohexane)	FS-30 (wt%)	X-100 (wt%)
1	0.487	3:7	1.5	0.05
2	0.589	3:7	1.5	0.05
3	0.638	3:7	1.5	0.05
4	0.715	3:7	1.5	0.05
5	0.745	3:7	1.5	0.05
6	0.770	3:7	1.5	0.05
7	0.825	3:7	1.5	0.05

#### 2.2.4. Influence of Surfactant Ratio

The results show that the surfactant can change the interfacial tension and destroy the balance between the three-phase interfacial tensions, thus affecting the internal interface morphology of Janus droplets. To investigate the impact of surfactants on Janus droplet structural color, we conducted 25 control experiments. These experiments varied the surfactant ratio while keeping the Janus droplet diameter-to-oil phase volume ratio constant at 0.569 mm and an n-hexane-to-perfluorohexane volume ratio of 3:7.

In order to explore the relationship between surfactants and interfacial tension and aperture diameter, the hanging drop method was used [43–45]. The interfacial tension under different surfactants was measured. First, the image of the hanging drop was obtained through experiments and converted into a 16-bit graph. Following the acquisition of the image, it was imported into MATLAB (Mathworks Inc., Natick, MA, USA). In this step, the needle diameter was provided as input, and the program carried out an automatic calibration of the pixel size. Subsequently, the Canny edge operator was applied to process the symmetrical line of the hanging drop, extracting the coordinates of X and Z. Finally, the 4-5 Runge-Kutta method was used to calculate the total arc length and the curvature of the lowest point, and the shape factor and the interface tension were calculated.

#### 2.2.5. Statistical Analysis

All data are presented as mean  $\pm$  one standard deviation (SD) of n samples for each experimental group. Groups were compared using one-way analysis of variance (ANOVA) to determine significance. Differences between groups were considered significant when  $p < 0.05$ .

### 3. Results and Discussion

#### 3.1. Structural Color of Janus Droplets

When white light is irradiated in the vertical direction, the structural color phenomenon of Janus droplets is observed by using an inverted fluorescence microscope (Eclipse Ti-U, Nikon, Tokyo, Japan) (as shown in Figure 3). The reflected light is emitted from the ring near the three-phase contact line of the Janus droplet, indicating that the color is caused by the interaction between light and matter in a single droplet (as shown in Figure 4). The refractive index of n-hexane surpasses that of perfluorohexane. Consequently, when light enters perfluorohexane, characterized by its elevated refractive index, it undergoes total internal reflection at the concave surface. This phenomenon leads to the generation of the structural color as multiple beams of light, each taking distinct paths due to the internal reflection and interfering with one another upon exiting.

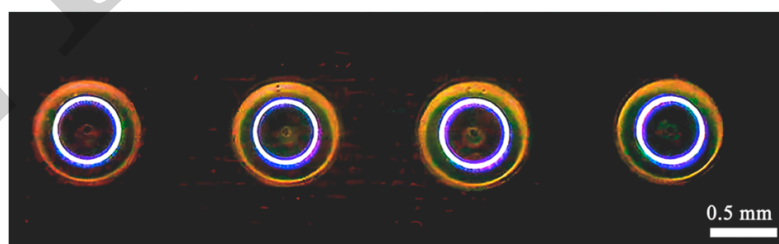


**Figure 3.** Janus droplets with vertical spatial orientation all show color apertures.

Therefore, the size of the structured color aperture of Janus droplets depends on the shape of the three-phase contact line. In this study, the objective was to attain precise control over the interface shape of Janus droplets and create structured color Janus droplets marked by uniform size, well-defined positioning, and precise spatial orientation. To accomplish this, we undertook a comprehensive series of comparative experiments. These experiments were designed to investigate the impact of specific variables—namely, the oil phase volume ratio of n-hexane and perfluorohexane, droplet size, and the proportion of nonionic surfactant—on the attributes and properties of the structured color apertures.

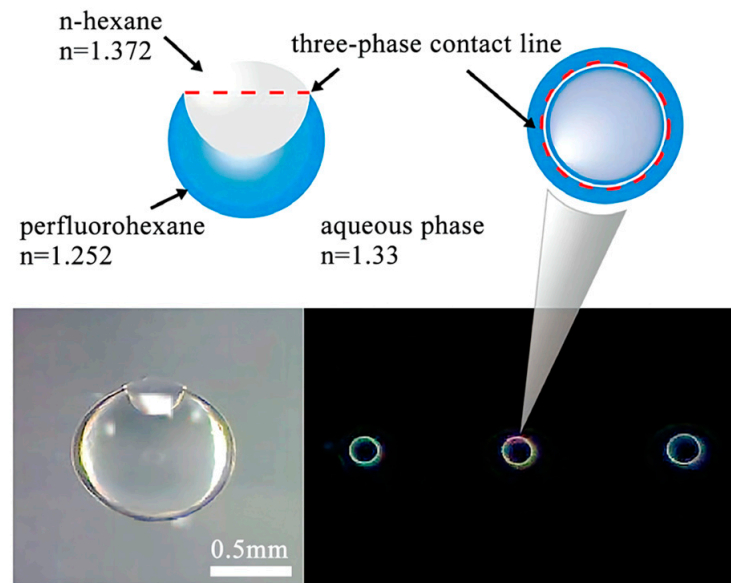


**Figure 4.** Janus droplets reflect color at the three-phase contact line.

### 3.2. Effect of Oil Phase Volume Ratio on Janus Droplets

The observation of Janus droplets was conducted using an inverted fluorescence microscope, which provided both top and side views of the results for seven experimental groups (as depicted in Figure 5). The figure reveals variations in the structured color apertures generated by Janus droplets with differing oil phase volume ratios. Notably, when the volume ratio is either 19:11 or 3:2, Janus droplets exhibit an absence of structured color apertures. Conversely, when the volume ratio is 11:19, the diameter of the structured color aperture in Janus droplets is notably smaller compared to when the ratio is 17:13. This discrepancy can be attributed to the constant total volume of droplets; lower volume ratios result in a reduced n-hexane content. Consequently, when Janus droplets establish a stable interface, the size of the three-phase contact line becomes smaller, leading to a reduced aperture diameter for the structured color. Conversely, larger volume ratios yield interface morphologies that do not meet the requirements for generating structural color, resulting in the absence of structured color apertures.

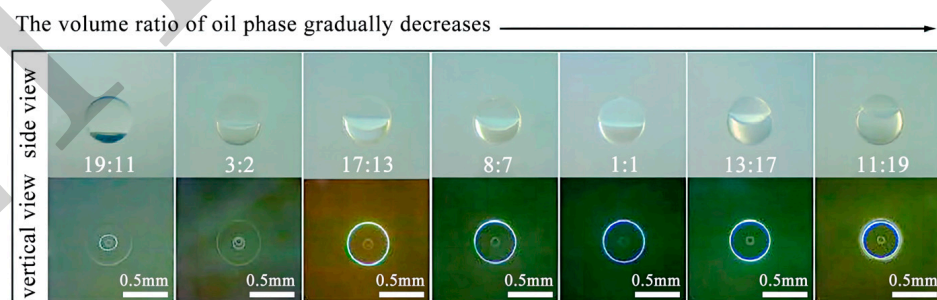


**Figure 5.** Comparison of structural color aperture of Janus droplets with different oil phase volume ratios.

From Figure 6, it can be seen that the oil phase volume ratio has an impact on the diameter of the structural color aperture. When the oil phase volume ratio is less than or equal to 17:13, Janus droplets will produce a structural color aperture, and their size will decrease as the volume ratio of n-hexane-to-perfluorohexane decreases. Therefore, the structural color aperture size of Janus droplets can be adjusted by adjusting the oil phase volume ratio.

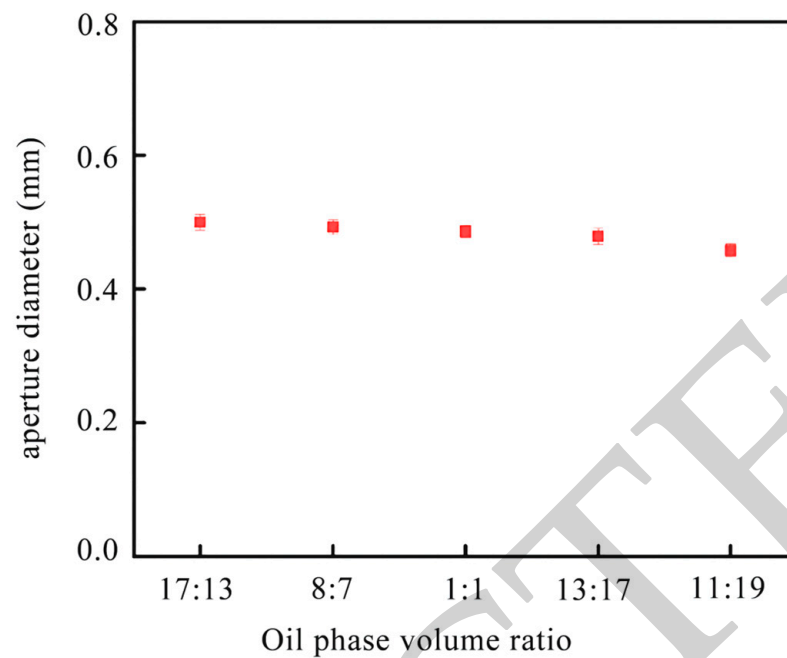


**Figure 6.** Relationship between oil phase volume ratio and structural color aperture diameter.

### 3.3. Influence of Droplet Size on Structure Color Aperture Diameter

Using an inverted fluorescence microscope to observe Janus droplets, a top and side view of seven experimental results were obtained (as shown in Figure 7). From the figure, it can be seen that the diameter of Janus droplets affects the diameter of the structural color aperture.

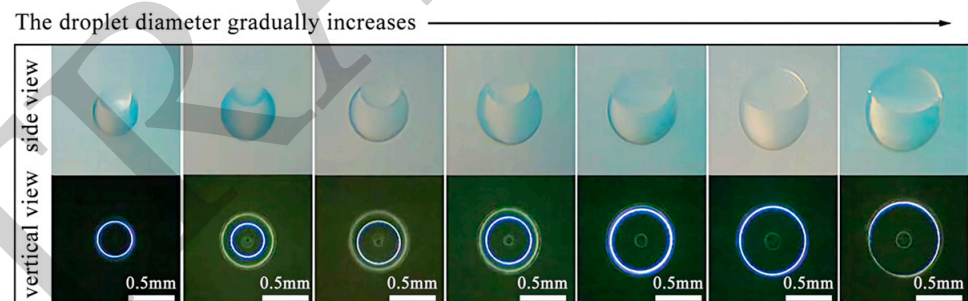


**Figure 7.** Comparison of structural color apertures of Janus droplets with different diameters.

As shown in Figure 8, the size of the Janus droplets is positively correlated with the size of the structural color aperture, meaning that as the size of the Janus droplets increases, the diameter of the structural color aperture also increases. In addition, when the droplet diameter is 0.745 mm, changes in interface morphology will lead to an increase in the size of the three-phase contact wire, and the diameter of the structural color aperture will also increase accordingly. However, changes in the diameter of droplets will not affect the generation of structural color apertures, as the interface morphology will not undergo significant changes.

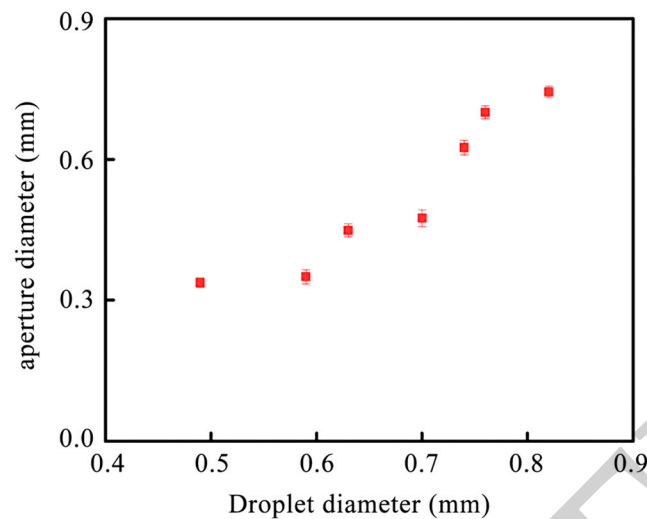


**Figure 8.** Relationship between droplet diameter and structured color aperture diameter.

### 3.4. Influence of Surfactant Ratio on Janus Droplets

The inverted fluorescence microscope was used to observe the Janus droplets, and the top view and side view of 25 groups of experimental results were obtained (as shown in Figure 9). It can be seen from the figure that the ratio of surfactant will affect the interfacial tension between the n-hexane and hydrogel and the perfluorohexane and hydrogel, thus changing the internal interface morphology of the Janus droplets and affecting the generation of the structured color aperture.

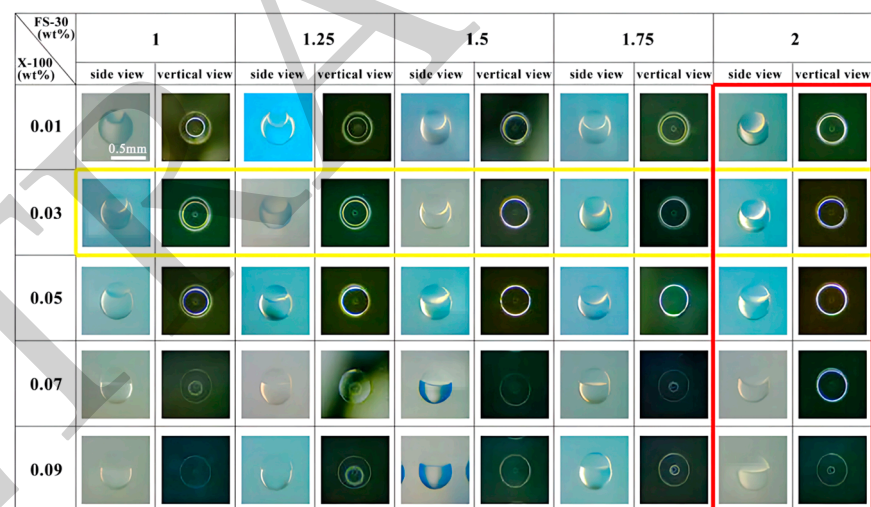


**Figure 9.** Comparison of structural color aperture of Janus droplets with different surfactant ratios, where the concentration of FS-30 in the red box is 2 wt%, and the concentration of X-100 in the yellow box is 0.03 wt%.

When X-100 is kept constant, such as 0.03 wt%, the diameter of the structured color aperture increases with the increase in FS-30 concentration (as shown in Figure 10a). This is because the interfacial tension between the perfluorohexane and carbomer hydrogel decreases with the increase in FS-30 concentration (as shown in Figure 10c). Similarly, when FS-30 is kept constant, such as 2 wt%, the diameter of the structured color aperture increases with the increase in X-100 concentration (as shown in Figure 10b). In addition, the diameter change of the structured color aperture is related to the change in the internal interface morphology of the Janus droplets. As the concentration of X-100 increases, the interfacial tension between the n-hexane and carbomer hydrogel decreases. Simultaneously,

the interfacial tension between the perfluorohexane and carbomer hydrogel increases. This leads to the formation of a larger three-phase contact line, as depicted in Figure 10d.

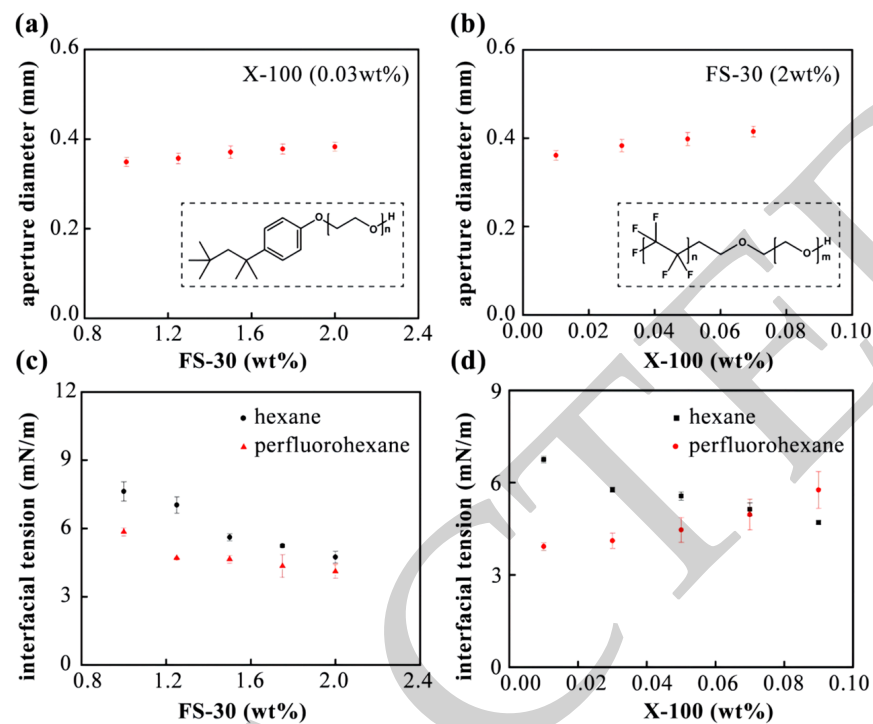


**Figure 10.** Influence of surfactants on interfacial tension and aperture diameter: (a) The effect of FS-30 on aperture diameter; (b) The effect of X-100 on aperture diameter; (c) The effect of FS-30 on interfacial tension; (d) The effect of X-100 on interface tension.

### 3.5. Patterned Printing

Microfluidic 3D droplet printing allows for the meticulous management of Janus droplet characteristics, encompassing size, spatial placement, and orientation. Additionally, it facilitates the precise modulation of the diameter of the structured color aperture through the manipulation of variables such as the oil phase volume ratio, droplet size, and surfactant concentration.

The G code of the pattern needs to be imported so it can be printed into a microfluidic 3D droplet printer. The 3D droplet printer reads the G code and transmits it to the control system, thereby controlling the feeding and moving mechanisms to feed materials and change the position of the printing nozzle and start printing. During the printing process, the microfluidic 3D droplet printer can dynamically adjust the feed rate of the microinjection pump, as well as the movement speed and pause time of the X/Y/Z axis, according to each instruction in the G code, thereby achieving control of the size and position of the Janus droplets.

The G code for the printing path of the cat- and the heart-shaped outlines is compiled using a text editor. Subsequently, microfluidic 3D droplet printing technology is employed to generate the color outline, depicted in Figure 11a,b. For the fish and heart models, the design is carried out using Solidworks, and the corresponding G code for the printing path is generated. Utilizing microfluidic 3D droplet printing technology once more, the color plane pattern is produced, as illustrated in Figure 11c,d. These color patterns exhibit remarkable brightness, clarity, and aesthetic appeal, showcasing the exceptional optical properties inherent in Janus droplets with structural color.

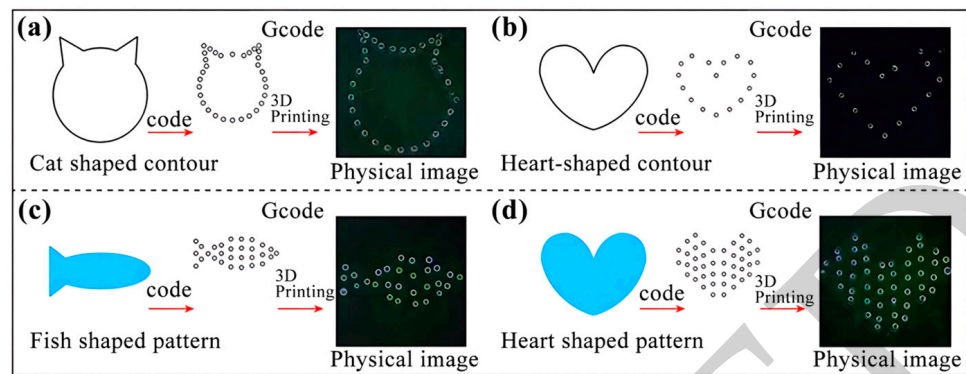


**Figure 11.** Patterned design of Janus droplets with structural color; (a) cat-shaped outline; (b) heart-shaped outline; (c) fish-shaped pattern; (d) heart-shaped pattern.

Moreover, Janus droplets, when suspended in a carbomer hydrogel, exhibit temperature-responsive characteristics. Precise temperature control allows for the deliberate manipulation of their phase separation, thereby facilitating the dynamic transition of the Janus droplets' structural color between a visible and concealed state, as illustrated in Figure 12. This captivating property presents an innovative avenue for advancing the development of anti-counterfeiting materials.

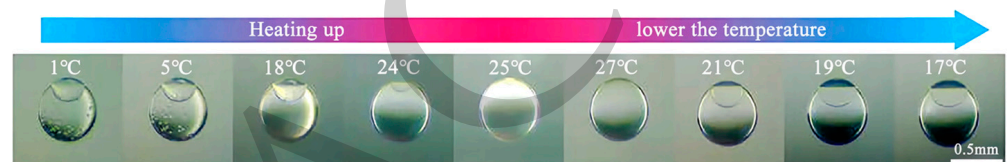


**Figure 12.** Temperature-sensitive characteristics of Janus droplets.

#### 4. Conclusions

For the printing material, this endeavor employed a carbomer hydrogel infused with a nonionic surfactant (FS-30/X-100) as the foundational substrate and a mixture of temperature-sensitive n-hexane and perfluorohexane. Microfluidic 3D droplet printing technology, combined with a temperature-induced phase separation method, successfully generated Janus droplets. The droplets were then characterized according to a consistent size and precise control over their spatial positioning and orientation. This study also engaged in an in-depth analysis of the underlying principles governing the production of structural color in Janus droplets. The influence of variables such as the volume ratio of the oil phase, droplet size, and surfactant composition was also explored.

Finally, the G code was compiled independently and generated the G code using printing software. The color patterns with specific shapes, such as the cat and fish shapes, were printed in the carbomer hydrogel. The degree of visualization was high. After that, the temperature was adjusted. The Janus droplets of structural color switched freely between a display and hidden state, which showed unique optical characteristics while broadening application paths.

**Author Contributions:** Conceptualization, C.W. and B.Y.; methodology, C.W. and H.J.; software, H.J. and H.Y.M.A.; validation, C.W., H.Y.M.A., A.S.M.M.F.S. and B.Y.; formal analysis, B.Y.; investigation, H.J. and H.Y.M.A.; resources, B.Y.; data curation, C.W.; writing—original draft preparation, C.W., H.Y.M.A. and A.S.M.M.F.S.; writing—review and editing, C.W. and B.Y.; visualization, C.W.; supervision, B.Y.; project administration, B.Y.; funding acquisition, C.W. and B.Y. All authors have read and agreed to the published version of the manuscript.

**Funding:** This research was funded by the Basic Science (Natural Science) Research Project of Jiangsu Province Higher Education Institutions [grant number 23KJD430014], the Innovative Science and Technology Platform Project of Cooperation between Yangzhou City and Yangzhou University, China [grant number YZ2020266], the “Green Yang Golden Phoenix Project” in Yangzhou City [grant number YZLYJF]H2021YXBS098], the National Natural Science Foundation of China [grant number 52075138], the Natural Science Foundation of the Jiangsu Higher Education Institutions of China [grant number 22KJB150050], the Jiangsu Agricultural Science and Technology Innovation Fund [grant number CX(21)3162], the Science and Technology Planning Project of Yangzhou City [grant number YZ2022180], and the Market Supervision Administration Science and Technology Fund of Jiangsu Province [grant number KJ2023076].

**Data Availability Statement:** Data sharing is not applicable to this article.

**Conflicts of Interest:** The authors declare no conflict of interest.

## References

1. Chen, J.; Liu, X.; Tian, Y.; Zhu, W.; Yan, C.; Shi, Y.; Kong, L.B.; Qi, H.J.; Zhou, K. 3D-Printed Anisotropic Polymer Materials for Functional Applications. *Adv. Mater.* **2022**, *34*, e2102877. [[CrossRef](#)]
2. Finny, A.S.; Popoola, O.; Andreescu, S. 3D-Printable Nanocellulose-Based Functional Materials: Fundamentals and Applications. *Nanomaterials* **2021**, *11*, 2358. [[CrossRef](#)] [[PubMed](#)]
3. Maslen, C.; Gholamipour-Shirazi, A.; Butler, M.D.; Kropacek, J.; Rehor, I.; Montenegro-Johnson, T. A New Class of Single-Material, Non-Reciprocal Microactuators. *Macromol. Rapid Commun.* **2023**, *44*, e2200842. [[CrossRef](#)] [[PubMed](#)]
4. Lu, F.; Neal, E.A.; Nakanishi, T. Self-Assembled and Nonassembled Alkylated-Fullerene Materials. *Acc. Chem. Res.* **2019**, *52*, 1834–1843. [[CrossRef](#)] [[PubMed](#)]
5. Wang, J.; Zhu, Z.; Liu, P.; Yi, S.; Peng, L.; Yang, Z.; Tian, X.; Jiang, L. Magneto-Responsive Shutter for On-Demand Droplet Manipulation. *Adv. Sci.* **2021**, *8*, e2103182. [[CrossRef](#)]
6. Guo, Q.; Li, Y.; Liu, Q.; Li, Y.; Song, D.P. Janus Photonic Microspheres with Bridged Lamellar Structures via Droplet-Confined Block Copolymer Co-Assembly. *Angew. Chem.* **2022**, *61*, e202113759. [[CrossRef](#)]
7. Qi, Y.; Zhou, C.; Qiu, Y.; Cao, X.; Niu, W.; Wu, S.; Zheng, Y.; Ma, W.; Ye, H.; Zhang, S. Biomimetic Janus photonic soft actuator with structural color self-reporting. *Mater. Horiz.* **2022**, *9*, 1243–1252. [[CrossRef](#)]
8. Liu, M.; Fu, J.; Yang, S.; Wang, Y.; Jin, L.; Nah, S.H.; Gao, Y.; Ning, Y.; Murray, C.B.; Yang, S. Janus Microdroplets with Tunable Self-Recoverable and Switchable Reflective Structural Colors. *Adv. Mater.* **2023**, *35*, e2207985. [[CrossRef](#)]
9. Sun, Q.; Hu, X.; Xu, B.; Lin, S.; Deng, X.; Zhou, S. Janus Charged Droplet Manipulation Mediated by Invisible Charge Walls. *Adv. Sci.* **2022**, *9*, e2204382. [[CrossRef](#)]
10. Zhang, H.; Wang, F.; Nestler, B. Janus Droplet Formation via Thermally Induced Phase Separation: A Numerical Model with Diffusion and Convection. *Langmuir ACS J. Surf. Colloids* **2022**, *38*, 6882–6895. [[CrossRef](#)]
11. Saqib, M.; Tran, P.A.; Ercan, B.; Erdem, E.Y. Microfluidic Methods in Janus Particle Synthesis. *Int. J. Nanomed.* **2022**, *17*, 4355–4366. [[CrossRef](#)]
12. Zhang, H.; Qu, T.; Wang, H.; Wu, W.; Lu, F.; Ou, J.; Zhu, G.; Gao, L.; Cheng, L. Preparation of asymmetric Janus hollow silica microparticle and its application on oily wastewaters. *Sci. Rep.* **2023**, *13*, 4135–4147. [[CrossRef](#)] [[PubMed](#)]
13. Kim, J.B.; Kim, J.W.; Kim, M.; Kim, S.H. Dual-Colored Janus Microspheres with Photonic and Plasmonic Faces. *Small* **2022**, *18*, e2201437. [[CrossRef](#)] [[PubMed](#)]
14. Raju, R.R.; Koetz, J. Pickering Janus Emulsions Stabilized with Gold Nanoparticles. *Langmuir ACS J. Surf. Colloids* **2022**, *38*, 147–155. [[CrossRef](#)]
15. Wei, X.; Cai, L.; Chen, H.; Shang, L.; Zhao, Y.; Sun, W. Noninvasive Multiplexed Analysis of Bladder Cancer-Derived Urine Exosomes via Janus Magnetic Microspheres. *Anal. Chem.* **2022**, *94*, 18034–18041. [[CrossRef](#)] [[PubMed](#)]
16. Montalbán, M.G.; Collado-González, M.; Lozano-Pérez, A.A.; Baños, F.G.D.; Vllora, G. Density and refractive index data of binary and ternary mixtures of imidazolium-based ionic liquids, n-hexane and organic compounds involved in the kinetic resolution of rac-2-pentanol. *Data Brief* **2018**, *19*, 134–144. [[CrossRef](#)] [[PubMed](#)]
17. Liu, Y.; Chen, F.; Guo, D.; Ma, Y. One-dimensional assembly of  $\beta$ -form anhydrous guanine microrods. *Soft Matter* **2021**, *17*, 1955–1962. [[CrossRef](#)] [[PubMed](#)]
18. Lee, Y.; Duy, P.K.; Chung, H. Incorporating Non-NIR Absorbing Agent into Packed Powder Samples in Diffuse Reflectance NIR Measurement to Improve Representation of Sample Composition and Accuracy of Concentration Determination. *Anal. Chem.* **2020**, *92*, 1016–1023. [[CrossRef](#)]
19. Teng, Z.; Wang, R.; Zhou, Y.; Kolios, M.; Wang, Y.; Zhang, N.; Wang, Z.; Zheng, Y.; Lu, G. A magnetic droplet vaporization approach using perfluorohexane-encapsulated magnetic mesoporous particles for ultrasound imaging and tumor ablation. *Biomaterials* **2017**, *134*, 43–50. [[CrossRef](#)]
20. Kikkawa, Y.; Tsuzuki, S. Analysis of intermolecular interactions of n-perfluoroalkanes with circumcoronene using dispersion-corrected DFT calculations: Comparison with those of n-alkanes. *Phys. Chem. Chem. Phys.* **2023**, *25*, 11331–11337. [[CrossRef](#)]

21. Morgado, P.; Garcia, A.R.; Martins, L.F.G.; Ilharco, L.M.; Filipe, E.J.M. Alkane Coiling in Perfluoroalkane Solutions: A New Primitive Solvophobic Effect. *Langmuir ACS J. Surf. Colloids* **2017**, *33*, 11429–11435. [[CrossRef](#)] [[PubMed](#)]
22. Warr, C.A.; Hinnen, H.S.; Avery, S.; Cate, R.J.; Nordin, G.P.; Pitt, W.G. 3D-Printed Microfluidic Droplet Generator with Hydrophilic and Hydrophobic Polymers. *Micromachines* **2021**, *12*, 91. [[CrossRef](#)] [[PubMed](#)]
23. Weigel, N.; Männel, M.J.; Thiele, J. Flexible Materials for High-Resolution 3D Printing of Microfluidic Devices with Integrated Droplet Size Regulation. *ACS Appl. Mater. Interfaces* **2021**, *13*, 31086–31101. [[CrossRef](#)] [[PubMed](#)]
24. Ying, Y.; Huang, Z.; Tu, Y.; Wu, Q.; Li, Z.; Zhang, Y.; Yu, H.; Zeng, A.; Huang, H.; Ye, J.; et al. A shear-thinning, ROS-scavenging hydrogel combined with dental pulp stem cells promotes spinal cord repair by inhibiting ferroptosis. *Bioact. Mater.* **2023**, *22*, 274–290. [[CrossRef](#)] [[PubMed](#)]
25. Hayati, F.; Ghamsari, S.M.; Dehghan, M.M.; Oryan, A. Effects of carbomer 940 hydrogel on burn wounds: An in vitro and in vivo study. *J. Dermatol. Treat.* **2018**, *29*, 593–599. [[CrossRef](#)]
26. Huang, Y.; Shi, F.; Wang, L.; Yang, Y.; Khan, B.M.; Cheong, K.L.; Liu, Y. Preparation and evaluation of *Bletilla striata* polysaccharide/carboxymethyl chitosan/Carbomer 940 hydrogel for wound healing. *Int. J. Biol. Macromol.* **2019**, *132*, 729–737. [[CrossRef](#)]
27. Lasky, J.A.; Thannickal, V.J. NOTCH-ing up Surface Tension in the Fibrotic Lung. *Am. J. Respir. Crit. Care Med.* **2023**, *207*, 235–236. [[CrossRef](#)]
28. Lin, J.J.; Kristensen, T.B.; Calderón, S.M.; Malila, J.; Prisle, N.L. Effects of surface tension time-evolution for CCN activation of a complex organic surfactant. *Environ. Science. Process. Impacts* **2020**, *22*, 271–284. [[CrossRef](#)]
29. Hsieh, T.L.; Law, S.; Garoff, S.; Tilton, R.D. pH-Dependent Interfacial Tension and Dilatational Modulus Synergism of Oil-Soluble Fatty Acid and Water-Soluble Cationic Surfactants at the Oil/Water Interface. *Langmuir ACS J. Surf. Colloids* **2021**, *37*, 11573–11581. [[CrossRef](#)]
30. Strickley, R.G.; Lambert, W.J. A review of Formulations of Commercially Available Antibodies. *J. Pharm. Sci.* **2021**, *110*, 2590–2608. [[CrossRef](#)]
31. Lbadaoui-Darvas, M.; Idrissi, A.; Jedlovsky, P. Computer Simulation of the Surface of Aqueous Ionic and Surfactant Solutions. *J. Phys. Chem. B* **2022**, *126*, 751–765. [[CrossRef](#)] [[PubMed](#)]
32. Tucker, I.M.; Burley, A.; Petkova, R.E.; Hosking, S.L.; Webster, J.R.P.; Li, P.X.; Ma, K.; Douth, J.; Penfold, J.; Thomas, R.K. Self-assembly in escin-nonionic surfactant mixtures: From micelles to vesicles. *J. Colloid Interface Sci.* **2022**, *626*, 305–313. [[CrossRef](#)] [[PubMed](#)]
33. Nguyen, T.X.D.; Razavi, S.; Papavassiliou, D.V. Janus Nanoparticle and Surfactant Effects on Oil Drop Migration in Water under Shear. *J. Phys. Chem. B* **2022**, *126*, 6314–6323. [[CrossRef](#)]
34. Lin, X.; Wu, H.; Zeng, S.; Peng, T.; Zhang, P.; Wan, X.; Lang, Y.; Zhang, B.; Jia, Y.; Shen, R.; et al. A self-designed device integrated with a Fermat spiral microfluidic chip for ratiometric and automated point-of-care testing of anthrax biomarker in real samples. *Biosens. Bioelectron.* **2023**, *230*, 115283. [[CrossRef](#)] [[PubMed](#)]
35. Yin, B.; Yue, W.; Sohan, A.; Wan, X.; Zhou, T.; Shi, L.; Qian, C.; Lin, X. Construction of a desirable hyperbolic microfluidic chip for ultrasensitive determination of PCT based on chemiluminescence. *J. Mater. Chem. B* **2023**, *11*, 1978–1986. [[CrossRef](#)] [[PubMed](#)]
36. Zeng, S.; Sun, X.; Wan, X.; Qian, C.; Yue, W.; Sohan, A.; Lin, X.; Yin, B. A cascade Fermat spiral microfluidic mixer chip for accurate detection and logic discrimination of cancer cells. *The Analyst* **2022**, *147*, 3424–3433. [[CrossRef](#)]
37. Yin, B.; Wan, X.; Sohan, A.; Lin, X. Microfluidics-Based POCT for SARS-CoV-2 Diagnostics. *Micromachines* **2022**, *13*, 1238. [[CrossRef](#)]
38. Yin, B.; Wan, X.; Qian, C.; Sohan, A.; Zhou, T.; Yue, W. Enzyme Method-Based Microfluidic Chip for the Rapid Detection of Copper Ions. *Micromachines* **2021**, *12*, 1380. [[CrossRef](#)]
39. Zhang, K.; Ren, Y.; Jiang, T.; Jiang, H. Flexible fabrication of lipophilic-hydrophilic micromotors by off-chip photopolymerization of three-phase immiscible flow induced Janus droplet templates. *Anal. Chim. Acta* **2021**, *1182*, 338955. [[CrossRef](#)]
40. Jiang, S.; Hu, Y.; Wu, H.; Zhang, Y.; Zhang, Y.; Wang, Y.; Zhang, Y.; Zhu, W.; Li, J.; Wu, D.; et al. Multifunctional Janus Microplates Arrays Actuated by Magnetic Fields for Water/Light Switches and Bio-Inspired Assimilatory Coloration. *Adv. Mater.* **2019**, *31*, e1807507. [[CrossRef](#)]
41. Bai, F.; Zhang, H.; Li, X.; Li, F.; Joo, S.W. Generation and Dynamics of Janus Droplets in Shear-Thinning Fluid Flow in a Double Y-Type Microchannel. *Micromachines* **2021**, *12*, 149. [[CrossRef](#)]
42. Sun, X.T.; Guo, R.; Wang, D.N.; Wei, Y.Y.; Yang, C.G.; Xu, Z.R. Microfluidic preparation of polymer-lipid Janus microparticles with staged drug release property. *J. Colloid Interface Sci.* **2019**, *553*, 631–638. [[CrossRef](#)]
43. Chen, C.M.; Chang, C.H.; Chao, C.H.; Wang, M.H.; Yeh, T.F. Biophysical and chemical stability of surfactant/budesonide and the pulmonary distribution following intra-tracheal administration. *Drug Deliv.* **2019**, *26*, 604–611. [[CrossRef](#)]
44. Millionis, A.; Antonini, C.; Jung, S.; Nelson, A.; Schutzius, T.M.; Poulikakos, D. Contactless Transport and Mixing of Liquids on Self-Sustained Sublimating Coatings. *Langmuir ACS J. Surf. Colloids* **2017**, *33*, 1799–1809. [[CrossRef](#)]
45. Li, H.; Fauquignon, M.; Haddou, M.; Schatz, C.; Chapel, J.P. Interfacial Behavior of Solid- and Liquid-like Polyelectrolyte Complexes as a Function of Charge Stoichiometry. *Polymers* **2021**, *13*, 3848. [[CrossRef](#)]

**Disclaimer/Publisher's Note:** The statements, opinions and data contained in all publications are solely those of the individual author(s) and contributor(s) and not of MDPI and/or the editor(s). MDPI and/or the editor(s) disclaim responsibility for any injury to people or property resulting from any ideas, methods, instructions or products referred to in the content.